Inorg. Chem. **2004**, *43*, 6922–6935

Local Structure and Charge Distribution in the UO_2–U_4O_9 System

Steven D. Conradson,*,† Dario Manara,‡ Franck Wastin,‡ David L. Clark,§ Gerard H. Lander,‡ Luis A. Morales,|| Jean Rebizant,‡ and Vincenzo V. Rondinella‡

Materials Science and Technology Division, Nuclear Materials and Technology Division, and Seaborg Institute for Transactinium Science, Los Alamos National Laboratory, Los Alamos, New Mexico 87544, and European Commission, JRC, Institute for Transuranium Elements, D-76125, Karlsruhe, Germany

Received February 26, 2004

Analysis of X-ray absorption fine structure spectra of UO_{2+x} for $x = 0$–0.20 (UO_2–U_4O_9) reveals that the adventitious O atoms are incorporated as oxo groups with U–O distances of 1.74 Å, most likely associated with U(VI), that occur in clusters so that the UO_2 fraction of the material largely remains intact. In addition to the formation of some additional longer U–O bonds, the U sublattice consists of an ordered portion that displays the original U–U distance and a spectroscopically silent, glassy part. This is very different from previous models derived from neutron diffraction that maintained long U–O distances and high U–O coordination numbers. UO_{2+x} also differs from PuO_{2+x} in its substantially shorter An–oxo distances and no sign of stable coordination with H_2O and its hydrolysis products.

Introduction

Uranium is the basis of one of the most complex metal oxide systems known.[1,2] Binary uranium oxides are of ongoing technological importance because of their use in nuclear fuels, their role in environmental migration, and their long-term storage issues. The scientific issues associated with uranium oxides have been sufficiently challenging to foster continuous efforts in the field for more than 60 years. Despite the ensuing body of work, our understanding of UO_2-UO_3 is far from complete. This is particularly true in the area of nonstoichiometric oxides, UO_{2+x}, where interstitial O atom mobility is rapid and reversible.[3] The scientific challenge is the identification of the chemical and structural mechanisms by which excess O is incorporated into the UO_{2+x}, how this influences the intermediate phases, and the comparison of this mechanism with related processes in other actinide oxide species, especially PuO_{2+x}.[4,5]

The light actinide elements, Th−Cm, adopt the cubic *Fm*3*m* fluorite type crystal structure for their AnO_2 compounds. The extraordinary stability of these cubic binary oxides is responsible for the existence of tetravalent dioxides of Pa, Am, Cm, and Cf despite the instability of valence (IV) of these elements in aqueous solution. Another aspect of this stability for those actinides that do support higher valences is the aforementioned ease with which mixed valence compounds are formed. In the oxidation of UO_2 to U_3O_8 (a process that continues to UO_3), U_4O_9 and U_3O_7 are both stable, coexisting intermediates that retain the U sublattice structure of UO_2 and are therefore slightly higher in density prior to the lattice expansion displayed by U_3O_8.[6] In fact, at least 16 distinct crystallographic oxide phases have been reported for uranium between the simple compositions of tetravalent UO_2 and hexavalent UO_3.[7] The addition of O atoms to UO_2 can therefore be tracked through the crystallographically identified U_4O_9, U_3O_7, and U_3O_8 intermediates

* To whom correspondence should be addressed E-mail: conradson@lanl.gov.
† Materials Science and Technology Division, Los Alamos National Laboratory.
§ Seaborg Institute for Transactinium Studies, Los Alamos National Laboratory.
‡ Institute for Transuranium Elements.
|| Nuclear Materials and Technology Division, Los Alamos National Laboratory.

(1) Weigel, F. In *The Chemistry of the Actinide Elements*; Katz, J. J., Morss, L. R., Seaborg, G. T., Eds.; Chapman and Hall: New York, 1986; Vol. 2.
(2) Haire, R. G.; Eyring, L. In *Handbook on the Physics and Chemistry of Rare Earths*; Gschneidner, K. A. J., Eyring, L., Choppin, G. R., Lander, G. H., Eds.; Elsevier Science B.V.: New York, 1994; p 413.
(3) Siegel, S.; Gallagher, F. X. *J. Inorg. Nucl. Chem.* **1970**, *32*, 3237.
(4) Haschke, J. M.; Allen, T. H.; Morales, L. A. *Science* **2000**, *287*, 285.
(5) Conradson, S. D.; Begg, B. D.; Clark, D. L.; Den Auwer, C.; Espinosa-Faller, F. J.; Gordon, P. L.; Hess, N. J.; Hess, R.; Keogh, D. W.; Morales, L. A.; Neu, M. P.; Runde, W.; Tait, C. D.; Veirs, D. K.; Villella, P. M. *Inorg. Chem.* **2003**, *42*, 3715.
(6) McEachern, R. J.; Taylor, P. *J. Nucl. Mater.* **1998**, *254*, 87.
(7) Allen, G. C.; Tempest, P. A. *Proc. R. Soc. London, Ser. A* **1986**, *406*, 325.

10.1021/ic049748z CCC: $27.50
Published on Web 09/28/2004

(but not U_2O_5, which is prepared by other means) before reaching the UO_3 endpoint.

Early models for UO_{2+x} proposed that the cubic interstitial sites in the fluorite lattice were randomly occupied by the added O atoms, thereby maintaining the observed cubic symmetry of the U sublattice that dominates the scattering of X-rays.[8] Subsequent neutron diffraction studies suggested that the excess O atoms enter the structure as clusters rather than individually and that the interstitial atoms are displaced from their ideal octahedral site, e.g., the eponymous "Willis structure."[9,10] The excess O atom enters the lattice at O′, which is displaced 1.09 Å along the ⟨110⟩ direction from the center of the interstitial hole in the fluorite lattice. The O′ atom ejects the two nearest O atoms from their normal lattice positions and displaces them approximately 1.33 Å along the ⟨111⟩ direction to generate O″ sites, leaving behind a vacancy V_O in the normal lattice site. The U atoms remain in their normal fcc positions. This leads to the ratio of numbers of atoms V_O:O′:O″ of 2:1:2 and is known as the 2:1:2 model. There is actually room enough to insert a second O′ atom without displacing any other normal O atoms, and the two O′ atoms are equivalent sites related by a 180° rotation. This leads to a model with the ratio of atoms V_O:O′:O″ 2:2:2, or the 2:2:2 model. Repeating this process along the line of V_O sites results in the 4:3:2 and higher defect clusters.

These highly ordered arrangements of defects are thought to organize first into these extended clusters, and then, U_4O_9 domains with much larger numbers of atoms evolve into the bulk compound as they grow; i.e., the local structure of the defects and U_4O_9 should be very similar.[7,11] The most recent descriptions give U−O distances (in addition to the ones for the UO_2 regions away from the defect) of around 2.22, 2.29, 2.35, 2.86, and 3.69 Å; the U−U distances are conserved because there are no U displacements. The next phase, U_3O_7, has new U−O distances of 2.28−2.34, 2.80−2.82, and 3.20−3.26 Å and also displays a retained U sublattice.[12] In these structural descriptions, one does not observe short U−O bond distances less than 2.2 Å, as observed in alkali metal uranates.[13,14] The increased charge is distributed over all of the neighboring U atoms because of the marginally shorter U−O′ distances and especially because the O″ atoms at the ends of the chains render their adjacent U atoms up the chain 9-coordinate.[14,15] This model proposes radically different behavior for the higher valence U than that typical of aqueous molecular complexes with O ligands where the increase in charge is concomitant with the formation of shorter U−O bond lengths (including uranyl) and reduced numbers of neighbors. In solids, the oblate geometry of the trans dioxo structure is generally conserved, although bridging oxo groups with greatly elongated bond lengths (up to 2.04 Å for the U(V) in $Ba_2U_2O_7$[16]) have been found in both higher oxides and actinates.[13] Other actinates show crystallographic evidence for symmetric, octahedral cation sites (KUO_3,[17] $BaUO_4$,[18] Ba_3UO_6[19]) with six identical U−O distances of around 2.15 Å. The "Willis" type model for the excess O incorporation mechanism was corroborated by an X-ray absorption fine structure (XAFS) measurement on $UO_{2.1}$.[20] What is not completely clear from the totality of these reports, especially in light of the crystallographic analysis of the ordered U_4O_9 phase (vide infra), is to what extent the analysis of the data may have preceded the model or, insofar as it was a reasonable guess based on the crystallographic evolution of the UO_y sequence, or vice versa.

In contrast to this structure proposed for UO_{2+x}, XAFS measurements on the crystallographically analogous PuO_{2+x} system have recently found the more conventional plutonyl speciation (PuO_2^+ or some solid state variant) and thus radically different behavior from that described in these models for UO_{2+x}.[5] The adventitious O occurs as easily identified PuO_2^{2+} oxo-type moieties with somewhat long Pu−O distances of 1.83−1.90 Å that, together with the X-ray absorption near edge structure (XANES), imply localized Pu(V+δ) sites. Furthermore, all of the compounds examined with the exception of those produced using a procedure that rigorously excluded any contact with H_2O, including those with $x \sim 0$, showed a multisite O distribution indicative of extremely stable Pu coordination with H_2O and/or its hydrolysis products. Despite these almost exhaustive structural studies of the binary U−O system, it is therefore nevertheless possible that the excess O could also form oxo groups so that the charge is localized on U(V) or (VI) sites if these were aperiodically distributed and thus essentially invisible to diffraction analysis. It is therefore of interest to determine to what extent the local and long range order do or do not (as is the case for PuO_{2+x}) coincide. If they do, and the excess O does not form oxo groups as it does in the higher valence coordination complexes, then the charge distribution mechanism for the U and Pu systems must differ radically.

Problems of this type are already evident in U_4O_9, the first recognized intermediate in the progression of UO_{2+x} ($x = 0.25$).[21] One group described the structure of U_4O_9 by dividing the UO_2 parts of the structure and the diffraction

(8) Alberman, K. B.; Anderson, J. S. *Angew. Chem.* **1949**, *61*, 416.
(9) Willis, B. T. M. *J. Chem. Soc., Faraday Trans.* **1987**, *83*, 1079.
(10) Willis, B. T. M. *J. Phys.* **1964**, *25*, 431. Willis, B. T. M. *Acta Crystallogr., Sect. A: Found. Crystallogr.* **1978**, *34*, 88.
(11) Allen, G. C.; Tempest, P. A. *J. Chem. Soc., Dalton Trans.* **1983**, 2673. Murray, A. D.; Willlis, B. T. M. *J. Solid State Chem.* **1990**, *84*, 52.
(12) Garrido, F.; Ibberson, R. M.; Nowicki, L.; Willis, B. T. M. *J. Nucl. Mater.* **2003**, *322*, 87.
(13) Morss, L. R. *J. Chem. Thermodyn.* **2002**, *34*, 229.
(14) Van den Berghe, S.; Verwerft, M.; Laval, J.-P.; Gaudreau, B.; Allen, P. G.; Van Wyngarden, A. *J. Solid State Chem.* **2002**, *166*, 320.
(15) Zachariasen, W. H. *J. Less-Common Met.* **1978**, *62*, 1.
(16) Cordfunke, E. H. P.; Ijdo, D. J. W. *J. Phys. Chem. Solids* **1988**, *49*, 551.
(17) Dickens, P. G.; Powell, A. V. *J. Mater. Chem.* **1991**, *1*, 137.
(18) Appel, H.; Bickel, M.; Melchior, S.; Kanellakopulos, B.; Keller, C. *J. Less-Common Met.* **1990**, *162*, 323.
(19) Cordfunke, E. H. P.; Booij, A. S.; Smit-Groen, V.; van Vlaanderen, P. *J. Solid State Chem.* **1997**, *131*, 341.
(20) Allen, G. C.; Tempest, P. A.; Garner, C. D.; Ross, I.; Jones, D. J. *J. Phys. Chem.* **1985**, *89*, 1334. Jones, D. J.; Roziere, J.; Allen, G. C.; Tempest, P. A. *J. Chem. Phys.* **1986**, *84*, 6075.
(21) Belbeoch, B.; Piekarski, C.; Perio, P. *Acta Crystallogr.* **1961**, *14*, 837. Belbeoch, B.; Boivineau, J. C.; Perio, P. *J. Phys. Chem. Solids* **1967**, *28*, 1267.

pattern from the distorted fraction and treating them separately.[22] The latter was then solved independently in the I_132 space group by quadrupling the lattice constant on all three axes. Resolving the overlaps of atoms resulting from this approach was not attempted (or at least reported), so that this process did not easily produce a unified depiction of the arrangement of atoms. However, in addition to the normal UO_2 pairs, 1.92 Å U−O and 3.49 Å U−U distances were reported, differing then from the alternative interpretation of the structure incorporating the 2:2:2 and 4:3:2 defect clusters. The accuracy of this structure has since been called into doubt because of problems with the assignment of the space group and the elimination of harmonics. More recent structure analyses of the β phase also utilized a $4 \times 4 \times 4$ expansion of the unit cell relative to UO_2 but in the $I\bar{4}3d$ space group.[23,24] The full analysis[23] found the O′ type atoms close positions originally postulated for the defect but also expanded the UO_{2+x} defect clusters into cuboctahedral structures in the multiplied unit cell, which they found was a common structural motif in hyperstoichiometric oxides and related compounds.[25] Subsequent reports on U_4O_9[24] and U_3O_7[26] corroborated this type of O ordering and identified additional displacements. In addition to those found in UO_2, there are prominent sets of U−O distances around 2.2−2.5, 2.8, and 3.5 Å that are close to those of the Willis structure and U−U distances of 3.75, 3.81, and 3.95−4.00 Å resulting from the U displacements. This includes U displacements that appear in the crystal structure but are not discussed in these papers, so that it is not clear if their claim that the U sublattice is conserved is intended to be rigorous or refers to the average structure. In fact, inspection of the structure recreated from the reported atom positions shows that it does not easily give the simple cuboctahedral clusters attributed to it. Although it is possible that these differences in the U_4O_9 structure found by the two groups result from incorrect analysis in the earlier one and also reflect different samples, they may also demonstrate the difficulty in the use of diffraction data in characterizing aperiodically disordered materials.

To address these issues, the local structure in a series of UO_{2+x} compounds for $x = 0.00-0.20$ has been determined by measurement and analysis of the U L_3 XAFS. This work constitutes a significant improvement over the earlier reports[20] not only because of the greater range and enhanced data quality resulting from improvements in experimental methods but also because a finer increment in O excess was achieved and our experience with the PuO_2 system made us aware of a wider variety of possible responses of the structure to the incorporation of the excess O.

Materials and Methods

Sample Preparation. The samples for XAFS measurements were prepared at the JRC Institute for Transuranium Elements in Karlsruhe, Germany. All operations through the mounting of the encapsulated samples in the cryostat, including storage and transport, were performed in N_2 or He atmospheres to prevent further oxidation or other changes to the samples.[6] The success of these procedures is demonstrated by the unequivocally monotonic changes in the spectra that correspond well with the values of x found immediately after preparation. Nuclear grade urania pellets, fabricated by Advanced Nuclear Materials Co., were powdered and annealed in a flux of 5% H_2 in Ar at 1273 K for 4 h to ensure that their composition was stoichiometric. The O/U atomic ratio was determined by thermogravimetric measurements from the change in the sample mass at full oxidation to U_3O_8 in air. The powder composition after annealing was $UO_{2.00\pm0.005}$. Hyperstoichiometric samples were prepared by treating the annealed $UO_{2.00}$ powder in an Al_2O_3 furnace at different temperatures under a CO/CO_2 flowing mixture of suitable composition, according to the $UO_{2\pm x}$ Ellingham diagram:[27] 15 h at 1473 K under 1:100 CO/CO_2 for $x = 0.05$, 15 h at 1573 K under 1:100 CO/CO_2 for $x = 0.08$, 15 h at 1323 K under 1:1000 CO/CO_2 for $x = 0.12$, 15 h at 1423 K under 1:1000 CO/CO_2 for $x = 0.17$, and 15 h at 1523 K under 1:1000 CO/CO_2 for $x = 0.20$. Samples were prepared for XAFS by grinding them into powders that were mixed with cellulose dried under vacuum at 55 °C and then pressing them into a pellet. The pellets were then sealed within Lucite holders with Stycast resin, stored for two months, and then shipped under inert atmosphere. This procedure routinely yields airtight containment of the samples. XRD analysis demonstrated that, except for some cellulose diffraction peaks, all the encapsulated samples were identical with their forms prior to the powdering operation. The lattice constant found for $U_{2.00}$ was 5.4706(1) Å, consistent with reported values. Due to the miscibility gap between UO_2 and U_4O_9, the diffraction patterns of samples with $x > 0$ show shoulders and then split peaks at room temperature corresponding to UO_2 and U_4O_9 ($a = 5.44$ Å at $x = 0.20$). The lattice parameters and relative areas for the two peaks are consistent with the O stoichiometry determined by thermogravimetric analysis and previous literature values. A detailed analysis of the diffraction patterns beyond that required to confirm the thermogravimetric analysis and preservation of the material through its enacapsulation is outside the scope of this paper. We note again that the thermogravimetric analysis, general characteristics of the diffraction patterns, and progression of the XAFS spectra are all consistent with the reported O stoichiometries.

Acquisition and Analysis of XAFS Spectra. All XAFS measurements were performed at the Stanford Synchrotron Radiation Laboratory, under dedicated operating conditions (3.0 GeV, 50−100 mA), on end station 11-2. Sample holders were attached to the coldfinger of a liquid N_2 cryostat so that the sample temperatures were near 80 K. Si [220] crystals were used to monochromate the beam. Harmonics were eliminated with a flat, Pt-coated mirror tilted to a cutoff energy of 20−25 keV. All spectra were recorded in fluorescence mode using a multielement Ge detector and digital amplifiers. A dead time correction of around 1 μs was made to adjust the absorption peak height to match that of the transmission data. This can also correct for self-absorption. Energy calibration was accomplished by measuring the spectrum of a Zr foil with a third ion chamber before the actual scan of the sample over the U edge. The first inflection point of the Zr foil was defined as 17999.35 eV. The fluorescence/I_0 (incident beam

(22) Masaki, N.; Doi, K. *Acta Crystallogr.* **1971**, *B28*, 785.
(23) Bevan, D. J. M.; Grey, I. E.; Willis, B. T. M. *J. Solid State Chem.* **1986**, *61*, 1.
(24) Lauriat, J. P.; Chevrier, G.; Boucherle, J. X. *J. Solid State Chem.* **1989**, *80*, 80.
(25) Bevan, D. J. M.; Greis, O.; Strahle, J. *Acta Crystallogr., Sect. A: Cryst. Phys. Diff. Theor. Gen. Crystallogr.* **1980**, *36*, 889. Bevan, D. J. M.; Lawton, S. E. *Acta Crystallogr., Sect. B: Struc. Sci.* **1986**, *42*, 55.
(26) Nowicki, L.; Garrido, F.; Turos, A.; Thome, L. *J. Phys. Chem. Solids* **2000**, *61*, 1789.
(27) Lindemer, T. B.; Besmann, T. M. *J. Nucl. Mater.* **1985**, *130*, 473.

Table 1. XANES Parameters[a]

sample	edge energy	peak energy	peak height	Δ(Gauss − arctan)[b]
$UO_{2.00}$	17163.1	17169.4	1.55	6.7
$UO_{2.05}$	17163.2	17169.7	1.49	7.0
$UO_{2.08}$	17162.9	17169.4	1.46	8.3
$UO_{2.12}$	17162.9	17169.6	1.43	10.5
$UO_{2.17}$	17163.2	17169.9	1.41	11.6
$UO_{2.20}$	17163.0	17169.9	1.37	13.2

[a] Edge inflection points and peak energies based on first inflection point of Zr metal = 17999.35. [b] Difference in eV between the Gaussian used to fit the high energy side of primary peak in the spectrum and the arctangent used to fit the absorption edge determined from curve-fits of XANES.

intensity through an ion chamber in front ot the sample) absorbance was normalized by offsetting it so that the value of a second-order polynomial fit through the pre-edge was zero and scaling it so that the value of a third-order polynomial fit through the region above the edge was unity at 17185 eV. The reported peak energies are the zeroes of the first derivative; the edge energies are the inflection points of the absorption edges. Differentiation was performed numerically. The precision of the results (Table 1) so obtained is much better than the ca. 0.8 eV interval between data points because it also depends on the much finer interval of the absorption data. The precision is thus derived from the accuracy of the energy determination and the error in the monochromator position. From our experience with duplicate samples, the accuracies of the tabulated energies for all spectra collected in a single experimental run are around 0.2−0.3 eV.

The extended X-ray absorption fine structure (EXAFS) was extracted from the spectra by first subtracting out the absorption edge using a sum of an arctangent and a Gaussian fit to the absorption edge and peak. A polynomial spline function was then fit to the remainder of the spectrum to approximate the smooth atomic absorption. The knot positions were optimized by minimizing the area of the Fourier transform modulus of the EXAFS from 0 to 1.1 Å. Substantial effort was made to use very similar polynomial spline parameters and obtain the same function for all spectra to minimize the effects of background artifacts on the curve-fitting results. During this process, E_0 was reset to 17172.0 eV, which not only is closer to the edge but also resulted in ΔE_0 values in the fits that are closer to 0. Metrical results in terms of N, the numbers of atoms in a shell, r, the U−O/U distances, and σ, the pairwise Debye−Waller factors, were obtained by curve-fits of the $\chi(k)$ data over the ranges depicted in the figures, which utilized the full spectral range available. Fourier transforms ($\chi(R)$) were performed over the same range, also using k^3 weighting to enhance the accuracy for the O shells, and a sine window. Pairwise U−O and U−U curve-fitting parameters were obtained using FEFF7.[28] The total spectrum was also calculated this way, and then it was scaled to give the best match to the experimental spectra. The number of shells used is the same as in Table 2 and therefore can vary among the samples. Fits were typically begun with nine shells, and the number was reduced if two shells either converged or destroyed each other. Most spectra displayed a feature that could be fit by an O shell at >3.6 Å that exhibits substantial overlap with the U shell. Because of this problem and insofar as a shell at this distance has no effect on the conclusions drawn from this study, this shell at the long distance was ignored in all but a few spectra. On the basis of the spectrum of $UO_{2.00}$, S_0^2 was set at 0.83 for the O shells and 0.79 for the U shell. After much trial and error, sets of constraints were found that were applied to all spectra. ΔE_0 was fixed at −2.0 eV for all O shells with U−O < 3.6 Å, and at 0 eV for the U shell, and allowed to float for the O shell at 4.47 Å. The Debye−Waller factor for the oxo shell was usually fixed at 0.045 Å. The Debye−Waller factors for the two or three largest O shells, which were typically the ones that compose the primary O shell with 2.15 < U−O < 2.45 Å, were allowed to float between 0.05 and 0.09 Å, although the range was smaller for some spectra. The Debye−Waller factors for all other O shells were set at the average value of these three or at 0.045−0.050 Å if a small value resulted in a significantly better fit. Curve-fits were first performed in which the total number of O atoms with 1.75 < U−O < 3.6 Å was fixed at eight. This is important because, whereas the curve-fits can optimize the parameters for a given model of the structure defined as the number of shells and their locations, selecting this model is much more arbitrary and, in determining the progressive changes in the structure with increasing x, it is essential that the curve-fits all begin with the same prototype structure. Because this large number of shells appeared to produce extra ones at locations such that their EXAFS waves canceled each other for some spectra, additional fits were performed in which this constraint was removed. This is discussed in the Results section. The Debye−Waller factors for the U and 4.47 Å O shells were allowed to float except when the resulting number of atoms was too large or small. Then, they were fixed at values that gave a number consistent with others in the particular set of compounds.

Reported errors in the curve fit results (Table 2) for N, r, and σ (even when these did not vary in the fit) were derived by calculating the difference in the least squares errors between a fit that included the wave in question and one that did not to get the contribution of that wave to the fit. Each parameter for that wave was then varied until the least squares error was higher than the optimum by 10% of this contribution. This provided a fair representation of the sensitivity of the fit to an individual parameter. However, insofar as a major source of error in this analysis is correlation among the parameters from not only two but also three and more waves, the actual uncertainties for some parameters may be significantly larger. The number of independent parameters for the $k = 2.70-14.95$ Å^{-1} and $R = 1.2-4.6$ fitting ranges for these experiments is 28.[29] If the curve-fitting parameters are unconstrained, then this is 2.8−5.6 degrees of freedom for each of the 5−10 crystallographic shells of atoms. Even by fixing ΔE_0's and coupling N and σ for the different shells, the number of parameters used in the curve-fits approaches the limit of the degrees of freedom in those spectra requiring the higher numbers of shells. As is usual in EXAFS, the distances and other information originating in the phase will be much more accurate than numbers of atoms, σ's, and amplitude-dependent results. One well-known effect in spectra such as these where the amplitudes in some regions are low because of destructive interference between overlapping waves is that the amplitudes of the individual waves in the fit can increase to highly unrealistic values because their sum is still small, especially if the σ's are allowed to float. This was controlled by the judicious use of constraints on σ's and total numbers of atoms, as described, but it nevertheless demonstrates the problems in determining actual numbers of atoms and, by extension, uncertainties. Numbers of atoms can vary by factors of two or more, compensated by inverse changes in σ or the parameters for other shells, with concomitant insignificant changes in the quality of the fit. It is essentially impossible to discern from the quality of a fit alone if the number of atoms in a given shell is equal to that found crystallographically and the distribution is merely wide but still harmonic, or whether

(28) Ankudinov, A. L.; Rehr, J. J. *Phys. Rev. B: Condens. Matter* **1997**, *56*, R1712.

(29) Stern, E. A. *Phys. Rev. B: Condens. Matter* **1993**, *48*, 9825.

Table 2. Crystallographic Distances and $k^3\chi(k)$ Curve-Fitting Results[a]

	U−O 1.7 Å	U−O 2.0 Å	U−O 2.2 Å	U−O 2.4 Å	U−O 2.6 Å	U−O 2.8 Å	U−O 2.9 Å	U−O 3.2 Å	U−O <3.5 Å	U	U−O 4.5 Å
crystal structure				2.36 8 atoms						3.85 12	4.52 24
Willis 222/234 defects			2.22	2.36		2.86			3.69	3.85	4.52
Masaki U_4O_9		1.92		2.36					U−U: 3.49	3.85	4.52
$UO_{2.00}$											
R	1.73 ± 0.02	1.94 ± 0.02		2.36 ± 0.02						3.88 ± 0.01	4.59 ± 0.02
N	0.4 ± 0.1	0.6 ± 0.2		7.6 ± 2.3						10.6 ± 2.7	11.0 ± 3.5
σ	0.045 ± 0.018	0.045 ± 0.010		0.074 ± 0.014						0.056 ± 0.007	0.071 ± 0.014
$UO_{2.05}$											
R	1.74 ± 0.01	1.94 ± 0.01		2.36 ± 0.02	2.58 ± 0.01					3.88 ± 0.01	4.57 ± 0.02
N	0.5 ± 0.1	0.5 ± 0.1		6.5 ± 1.9	0.5 ± 0.2					8.5 ± 2.1	7.0 ± 2.2
σ	0.045 ± 0.095	0.045 ± 0.006		0.076 ± 0.014	0.045 ± 0.005					0.056 ± 0.007	0.057 ± 0.013
$UO_{2.08}$											
R	1.72 ± 0.02	1.98 ± 0.02	2.24 ± 0.01	2.38 ± 0.01	2.55 ± 0.02	2.77 ± 0.02	2.96 ± 0.02	3.22 ± 0.01	3.44 ± 0.01	3.88 ± 0.01	
N	0.3 ± 0.1	0.6 ± 0.2	2.1 ± 0.6	4.2 ± 1.1	1.6 ± 0.5	0.7 ± 0.2	0.6 ± 0.1	0.6 ± 0.2	0.5 ± 0.2	6.6 ± 1.6	
σ	0.045 ± 0.016	0.095 ± 0.017	0.045 ± 0.014	0.045 ± 0.013	0.045 ± 0.015	0.045 ± 0.016	0.045 ± 0.010	0.045 ± 0.006	0.045 ± 0.006	0.060 ± 0.006	
$UO_{2.12}$											
R	1.73 ± 0.02	1.97 ± 0.02	2.23 ± 0.01	2.38 ± 0.01	2.52 ± 0.02		2.96 ± 0.02	3.20 ± 0.01	3.43 ± 0.01	3.88 ± 0.01	
N	0.4 ± 0.1	0.7 ± 0.2	1.9 ± 0.5	3.2 ± 0.9	1.1 ± 0.3		0.6 ± 0.2	0.8 ± 0.2	0.8 ± 0.3	5.7 ± 1.4	
σ	0.045 ± 0.016	0.095 ± 0.017	0.045 ± 0.014	0.045 ± 0.013	0.047 ± 0.015		0.047 ± 0.016	0.045 ± 0.008	0.045 ± 0.0208	0.064 ± 0.006	
$UO_{2.17}$											
R	1.73 ± 0.01		2.25 ± 0.01	2.40 ± 0.01	2.56 ± 0.02		2.93 ± 0.01		3.51 ± 0.03	3.88 ± 0.01	4.45 ± 0.01
N	0.3 ± 0.1		1.9 ± 0.5	2.6 ± 0.7	0.8 ± 0.3		0.5 ± 0.2		2.2 ± 0.7	2.3 ± 0.5	4.5 ± 1.3
σ	0.045 ± 0.007		0.045 ± 0.014	0.045 ± 0.014	0.045 ± 0.015		0.045 ± 0.010		0.116 ± 0.019	0.034 ± 0.010	0.040 ± 0.013
$UO_{2.20}$											
R	1.76 ± 0.01		2.26 ± 0.02	2.42 ± 0.02			2.90 ± 0.01	3.11 ± 0.01		3.88 ± 0.009	4.52 ± 0.01
N	0.3 ± 0.1		1.8 ± 0.5	1.9 ± 0.6			0.8 ± 0.2	0.6 ± 0.2		2.5 ± 0.6	2.2 ± 0.7
σ	0.045 ± 0.007		0.057 ± 0.013	0.057 ± 0.013			0.045 ± 0.009	0.045 ± 0.006		0.050 ± 0.007	0.045 ± 0.013

[a] *R* = U−O/U distance. *N* = number of atoms in shell. σ = Debye−Waller factor.

the distribution is anharmonic, or if an actual split into a multisite distribution gives a lower effective number for a particular shell. The emphasis in the analysis is therefore on using means in addition to curve-fits to interpret the spectra. These include the direct comparisons of real parts and moduli of the transforms for identification of the oxo groups and the use of the composite partial radial distribution functions (rdf) instead of the values for individual shells.[30]

Results

X-ray Absorption Near Edge Spectra and Changes in the U Charge. The energies of the inflection point/edge energy and the absorption peak increase with increasing valence because the higher charge on the cation raises the electron binding energy.[31] The exception to this trend is that on going from An(IV) to actinyl(V) the edge energy decreases, probably because the highly covalent character of the oxo bonds in AnO_2^+ diminishes the actual charge on the metal. For valences ≥ V, however, the changes in geometry accompanying the formation of the various dioxo, tetraoxo, and actinate geometries are identifiable from the XANES.[14,31−34] On going from An(IV) to (V, VI), a shoulder appears on the high energy side of the main peak. The peak undergoes a substantial decrease in amplitude in association with the transformation from the spherically symmetric geometry of the lower valence to the oblate shape of the typical trans dioxo moiety with its two distinct oxo and equatorial bond lengths. Similarly, the more symmetric actinate geometry apparently gives a split primary peak that is somewhat lower on the low energy side.[14,33] This feature originates in a strong multiple scattering or outer well resonance. It is absent or greatly diminished in the similarly spherically symmetric An(III, IV) geometries most likely because of the expanded bond and path lengths. The most notable aspects of the energies associated with these UO_{2+x} spectra on going from $x = 0$ to 0.20 are the virtual absence of any shift in the edge energy and a ∼0.5 eV increase in peak energy (Table 1). Of these, the peak energy is a more consistent marker for changes in the charge because the edge energy is more sensitive to alterations in the shape of the peak.[31] If the charge on the U is localized, then the 20% U(VI) for $x = 0.20$ would dictate a 2.5 eV difference between the spectra of the UO_2 and the U(VI) species in UO_{2+x}. This is somewhat high compared with other An(IV, VI) pairs, but we have recently reported that other structural parameters

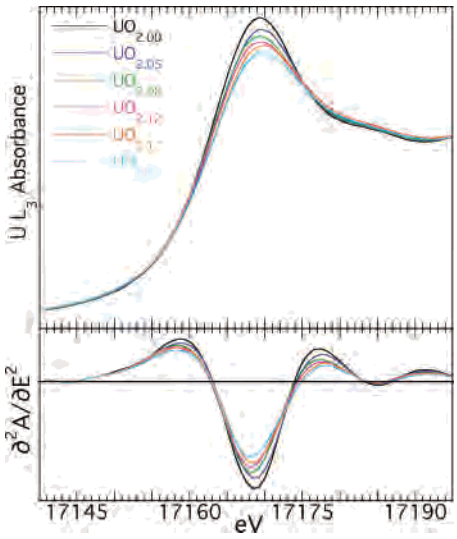

Figure 1. U L_3 XANES spectra of indicated samples (upper) and second derivatives of the same spectra (lower).

can also contribute to XANES energy shifts in PuO_{2+x}.[5,35] Since there would be little if any shift or even a negative one for U(V)−oxo if its XANES behaves like other actinides, this shift is indicative of the formation of the VI state.

A quantitative method for determining the relative amounts of each valence in U(IV, VI) mixtures has been demonstrated on the basis of the difference in energy between an arctangent used to fit the edge and a Gaussian used to fit the high energy asymmetry of the main peak.[32] The success of this technique must originate in a consistent difference between the shape of the spectra of the U(IV) and (VI) species analyzed with this technique.[32] The application of this procedure to these UO_{2+x} spectra produced both satisfactory fits and a monotonic progression in the difference between the second Gaussian and the edge energies (Table 1). The energy shifts so determined are, however, more than twice as large as those found previously over this relatively small fractional change in the U(IV/VI) ratio. This probably indicates that the higher valence U speciation in this system differs from the typical U(VI) trans dioxo structure of the meta-autunite that generated the original curve. Changes in peak shape that affect the peak amplitude have been observed in PuO_{2+x}.[31,35]

What is most unequivocally observed in the XANES of these samples is an almost linear decrease in the intensity of the main peak with increasing x (Figure 1), a simple effect that is not necessarily observed for PuO_{2+x}. There is also some softening or broadening on the high energy side so that, following an isosbestic point at 17176 eV, the amplitude at around 17180 eV goes up when that of the peak goes down. A decrease in the amplitude of the peak could result from some kinds of disorder,[36] although there are also examples of the inverse in the PuO_{2+x} system.[5,31] Analogous

(30) Tyson, T. A.; de Leon, J. M.; Conradson, S. D.; Bishop, A. R.; Neumeier, J. J.; Roder, H.; Zang, J. *Phys. Rev. B: Condens. Matter* **1996**, *53*, 13985.
(31) Conradson, S. D.; Abney, K. D.; Begg, B. D.; Brady, E. D.; Clark, D. L.; Den Auwer, C.; Ding, M.; Dorhout, P. K.; Espinosa-Faller, F. J.; Gordon, P. L.; Hess, N. J.; Hess, R. F.; Keogh, D. W.; Lander, G. H.; Lupinetti, A. J.; Neu, M. P.; Palmer, P. D.; Paviet-Hartmann, P.; Reilly, S. D.; Runde, W. H.; Tait, C. D.; Veirs, D. K. Wastin, F. *Inorg. Chem.* **2004**, *43*, 116.
(32) Morris, D. E.; Allen, P. G.; Berg, J. M.; Chisholm-Brause, C. J.; Conradson, S. D.; Donohoe, R. J.; Hess, N. J.; Musgrave, J. A.; Tait, C. D. *Environ. Sci. Technol.* **1996**, *30*, 2322. Conradson, S. D. *Appl. Spectrosc.* **1998**, *52*, A252.
(33) Den Auwer, C.; Simoni, E.; Conradson, S. D.; de Leon, J. M.; Moisy, P.; Beres, A. *C. R. Acad. Sci., Ser. IIc: Chim.* **2000**, *3*, 327.
(34) Williams, C. W.; Blaudeau, J. P.; Sullivan, J. C.; Antonio, M. R.; Bursten, B.; Soderholm, L. *J. Am. Chem. Soc.* **2001**, *123*, 4346.
(35) Conradson, S. D.; Begg, B. D.; Clark, D. L.; Den Auwer, C.; Ding, M.; Dorhout, P. K.; Espinosa-Faller, F. J.; Gordon, P. L.; Haire, R. G.; Hess, N. J.; Hess, R. F.; Keogh, D. W.; Morales, L. A.; Neu, M. P.; Paviet-Hartmann, P.; Runde, W.; Tait, C. D.; Veirs, D. K.; Villella, P. M. *J. Am. Chem. Soc.*, in press.
(36) Rothe, J.; Denecke, M. A.; Neck, V.; Muller, R.; Kim, J. I. *Inorg. Chem.* **2002**, *41*, 249.

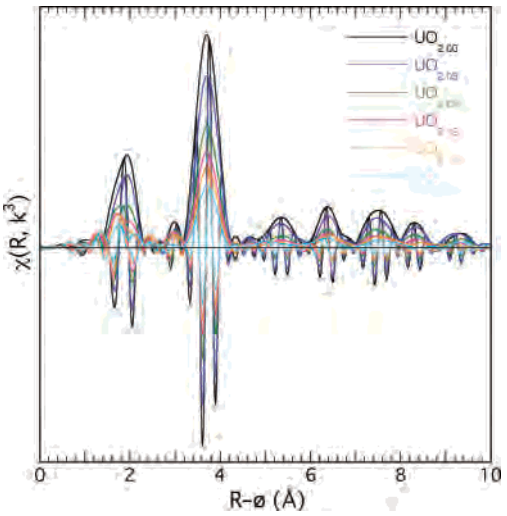

Figure 2. Modulus and real part of Fourier transforms of k^3-weighted EXAFS spectra of indicated samples. Transformation was performed over the range $k = 2.70-14.95$ Å^{-1}.

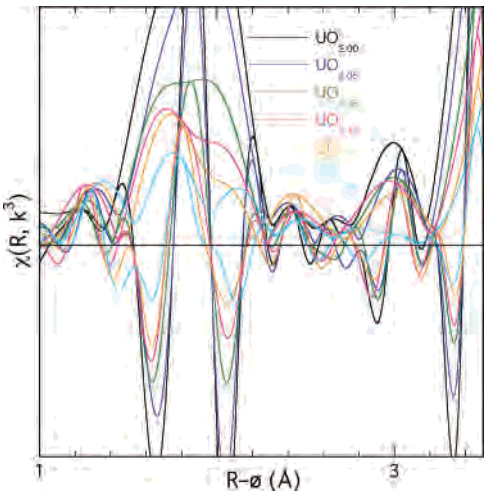

Figure 3. Expansion of the U−O nearest neighbor contribution region from Figure 2. As x increases, changes in both the modulus and real part that are not simply linear reductions of the original spectra are clearly observed (see text for discussion).

to the spectra of PuO_{2+x}, the primary change in the spectra is an asymmetric broadening of the peak and not a simple energy shift or change in amplitude. This broadening is manifested in the combination of concomitant fixed edge energy and, as x increases, increase in peak energy, decrease in amplitude at the peak, and increase in amplitude on the high energy side of the peak. This increase in the width of the peak is why the edge energy remains constant even as x increases. It also shows that the peak energy is a better metric for the actual energy of the XANES, which therefore increases toward U(VI) with increasing x. By analogy with Pu and Np, U(V) would produce a constant or even lower energy for the XANES. This change in shape would also be the reason the differences between the arctangent and second Gaussian energies in the edge fits are larger than those generated from the UO_2-meta-autunite Beers Law line. Although for these UO_{2+x} spectra the direction of the trend is the same, implying a similar increase in the U charge, the values of the energy shifts differ because the shape of the spectrum of the U(VI) species in UO_{2+x} is not the same as that of meta-autunite.

These characteristics show that the incorporation of excess O over this range of x engenders a single process with respect to modifications of the structure and that it is coupled to an increase in the average charge of the U that most likely produces a U(IV, VI) mixture where the U(VI) species gives a spectrum shaped differently from that of typical trans dioxo compounds. Additional details of the modifications to the U speciation that cause this change in the XANES require recourse to the EXAFS portion of the spectrum.

EXAFS Spectra. Inspection of the $\chi(R)$ spectra reveals aspects of the changes to the average local structure of the target element, in this case as a function of increasing O content. The $\chi(R)$ spectra (Figure 2) show the U environment of UO_{2+x} undergoing one general and one more specific process through this range in x. At $x = 0$, the spectrum is that of the cubic, fluorite-type oxide. The first peak is the contribution of the eight nearest neighbor O atoms (Table 2), well separated from the more distant second nearest neighbor metal peak whose larger amplitude reflects its higher Z and 12 atoms. Regular features from the well ordered, extended structure subsequently continue out through very high R. As x increases, the amplitudes of all of the peaks decrease monotonically, indicative of diminished order via displacements of the U and O atoms from their lattice sites coupled to the incorporation of the nonstoichiometric O atoms into interstitial, essentially defect sites. What is unexpected in this process is that this loss of amplitude is similar in proportion for all R; the spectrum of the $x = 0.20$ sample displays peaks at $R = 7.5$ and even 9.4 Å with intensities relative to the largest peak near $R = 3.8$ Å comparable to those for $x = 0.0-0.05$. Random disorder would result in faster loss of spectral amplitude at higher R as the material became glassy. This suggests that the defects tend to cluster so that a significant fraction of the lattice retains its original UO_2 structure even as the U_4O_9 composition is approached.

The nearest neighbor O peak is the only large feature displaying any behavior that differs from this simple loss of amplitude. As x increases, a shoulder on the low R side becomes more prominent relative to the rapidly diminishing primary O peak. At $x = 0.12$ the peak on the low R side is larger than the peak at the original position, and finally, these two features are resolved at higher x. This implies that, in contrast to the other structural features, the underlying nearest neighbor O distribution is not simply becoming broader but is splitting into a multisite distribution.

A closer examination of this feature and its environs (Figure 3) shows some additional aspects of this trend. The most significant observation is that the adjacent features are not responding proportionately or linearly to the increase in x. The two small peaks near $R = 2.6$ and 2.8 Å for $x \leq 0.05$ merge into a single one for $x \geq 0.08$. The modulus of the peak near $R = 3$ Å diminishes by only half at $x = 0.17$, and then vanishes in association with a radical change to the real component at lower R. The peak at $R = 2.4$ Å attains its

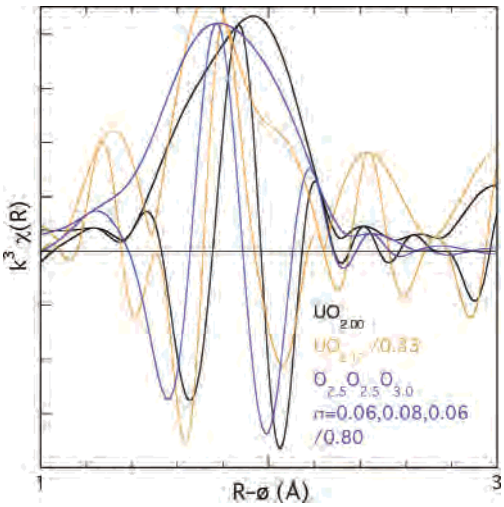

Figure 4. Multiplying the $UO_{2.17}$ spectrum from Figure 3 by a factor of 3 increases the amplitude of its primary nearest neighbor O contribution to match that of the $UO_{2.00}$ spectrum, showing the overwhelming significance of the small features near $R = 1.3$ and 2.4 Å relative to this main peak. The spectrum of an O distribution containing some of the characteristics found by curve-fits for the $UO_{2.17}$ sample, composed of 2.5 O at 2.21 Å ($\sigma = 0.06$ Å), 2.5 O at 2.29 Å ($\sigma = 0.08$ Å), and 3.0 O at 2.36 Å ($\sigma = 0.06$ Å), normalized to the same height by multiplying it by 1.25, shows that disorder-induced sidelobes cannot be proportionately larger than in the spectrum of the fully ordered structure so that these new spectral features (at $R = 1.3$ and 2.4 Å) must originate in new shells of atoms.

maximum amplitude at $x = 0.17$. At $R = 1.3$ Å, there is no resolved feature at $x = 0$; immediately following at $x = 0.05$, there is a large peak whose amplitude remains relatively constant but whose position shifts to higher R with increasing x. There are also concomitant changes in the real part; the local maximum near $R = 1.4$ Å at $x = 0$ undergoes a continuous decrease from positive to negative and shifts in position to near $R = 1.6$ Å at $x = 0.20$. These changes raise the issue of whether the loss of amplitude of the primary peak simply reflects increasing disorder or if new structural features are appearing in the spectrum as the composition changes. Relative to the first shell O peak in the $x = 0$ spectrum, the small features would merely be side lobes and the peak at $R = 3.0$ Å would reflect the complicated U−U amplitude with its Ramsauer−Townsend resonance at lower k. However, because the amplitudes of these modulus peaks do not decrease in parallel with the primary ones their relative significance is enhanced. In the $x = 0.17$ spectrum, they are of the same order as the main O contribution, and at $x = 0.20$, the $R = 1.4$ Å peak is actually slightly larger than the one near 2.1 Å. Multiplying the $x = 0.17$ $\chi(R)$ spectrum by a factor of 3 to make the amplitude of the O peak the same as that in the $x = 0$ spectrum (Figure 4) shows this effect. The large shift in the real component confirms changes in the structure. If these spectra were analyzed in isolation from the others, these spectral features would be unequivocally assigned to structural components because of their size relative to the diminished peak at the original position.

To test whether the disorder in the O shell could reduce the primary amplitude without affecting the magnitude of the side lobes, rendering them large as disorder reduces the peak height of the main structural feature, a series of simulations were run in which various types of U−O disorder were introduced. In all the different configurations examined, including the one that was closest to the data where three O shells at 2.21, 2.29, and 2.36 Å were summed (Figure 4), the side lobes were always closely correlated with the main peak so that it was never possible to raise the relative amplitude of the side lobes above that already occurring in the $x = 0$ spectrum. This confirms the interpretation of the experimental spectral behavior as representing changes in distinct shells and not as the result of increased disorder in the U−O distribution. There are thus obvious changes to the nearest neighbor O distribution, most likely including both ordered and disordered ones, some of which are not continuous.

Curve-Fitting Determination of Metrical Parameters. Extracting the local structure in disordered materials by curve-fitting is difficult because although the fits optimize the parameters for the neighbor shells, they do not unambiguously determine how many shells there are nor their locations. In comparing a series of related compounds, such as in this work, the most significant but also most difficult analysis issue is distinguishing when a new feature actually arises in the structure. Rather than make arbitrary judgments on this, all of the spectra were initially fit with the same trial structure that included eight O shells with U−O < 3.5 Å. If these converged with each other or if their amplitudes went to zero or otherwise became physically unrealistic, then they were removed from the fits and it could be safely assumed that the actual structures were simpler than this initial model. (Significant residuals in the fits called for the addition of more shells in some cases.) There were, however, also instances when a shell remained in the fit and gave reasonable metrical parameters but is nevertheless unlikely to indicate an actual structural feature because of very low amplitude or parameter correlation or poor quality of fit where it made its contribution. The most notable of these is the putative oxo shell, which is discussed below. The significance of a given shell in the fit and the likelihood that it is real can be evaluated by noting its amplitude relative to that of other shells and in the total spectrum, the correspondence between the data and fit, and its effect on the radial structure function determined by the fit.

Two types of curve-fits were performed using different models for the U−O distribution. This is critical because the curve-fitting procedure can only refine the particular model used: it is unable to introduce features that are not present initially nor can it necessarily determine if an included shell is extraneous. The first set of fits fixed the total number of O atoms with U−O < 3.6 Å to eight. This assumes that the average number of nearest neighbors does not vary significantly from that found in the starting $UO_{2.00}$, and that these atoms are arranged so that they all make distinct, identifiable contributions to the spectrum. This constraint gave good fits, but for some spectra these fits included several small shells with U−O > 2.5 Å that were separated by distances that maximized the destructive interference between them. This substantially reduced their overall combined amplitude in the spectrum. To test whether these were artifacts of the constraint, a second set of fits was performed in which the total number of O atoms was

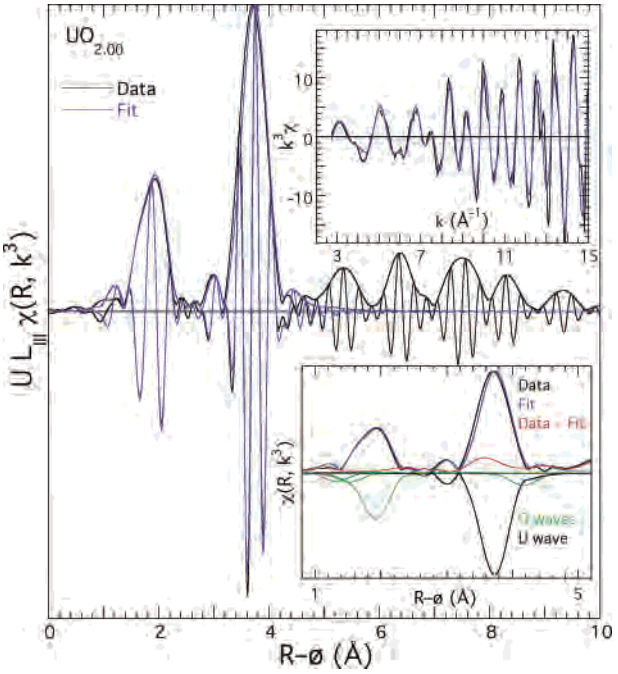

Figure 5. $k^3\chi(R)$ EXAFS of $UO_{2.00}$ and five shell O, O, O, U, O fit. The modulus and real part of the transform of both the data and fit are shown. The insets show the $k^3\chi$ spectrum overlaid with the curve-fit (top) and the (bottom) moduli of the data, fit, difference between the data and fit, and the individual contributions to the fit (inverted for clarity).

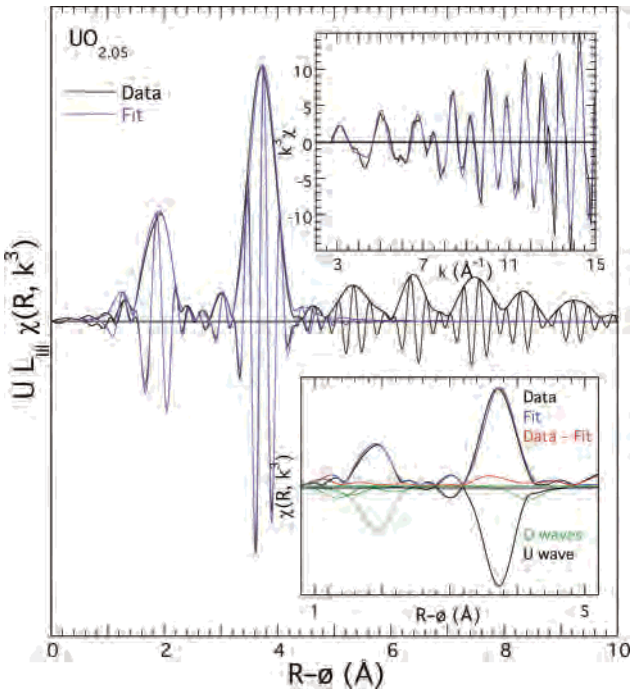

Figure 6. $k^3\chi(R)$ of the EXAFS of $UO_{2.05}$ and six shell fit to the spectrum of $UO_{2.05}$. The modulus and real part of the transform of both the data and fit are shown. The insets show the $k^3\chi$ spectrum overlaid with the curve-fit (top) and the (bottom) moduli of the data, fit, difference between the data and fit, and the individual contributions to the fit (inverted for clarity). The vertical scale of the main plots is identical to those in Figure 5, and the vertical scales of the two insets are adjusted so that they are filled by the data.

not fixed (Table 2 and Figures 5−10). In these fits, these interfering shells were not needed to obtain good fits, implying that these shells are not actually part of the structure but merely a response to the fixed number constraint.

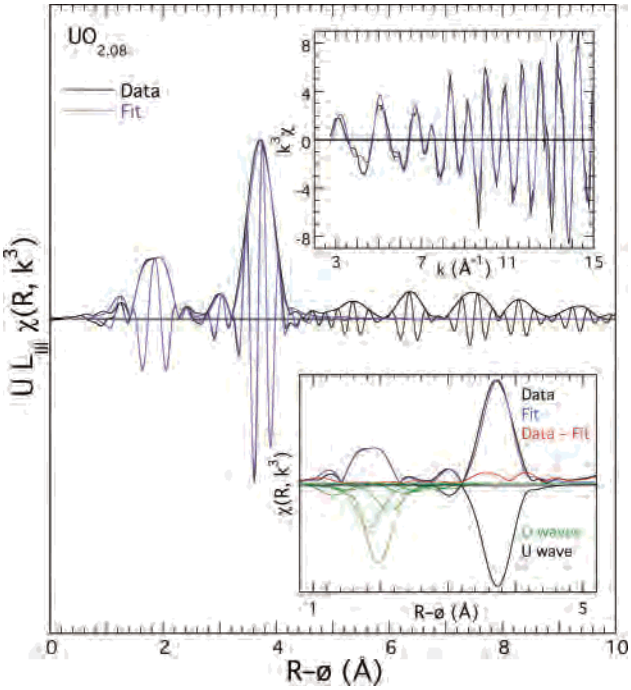

Figure 7. $k^3\chi(R)$ of the EXAFS of $UO_{2.08}$ and 10 shell fit to the spectrum of $UO_{2.08}$. The layout is identical to Figure 6.

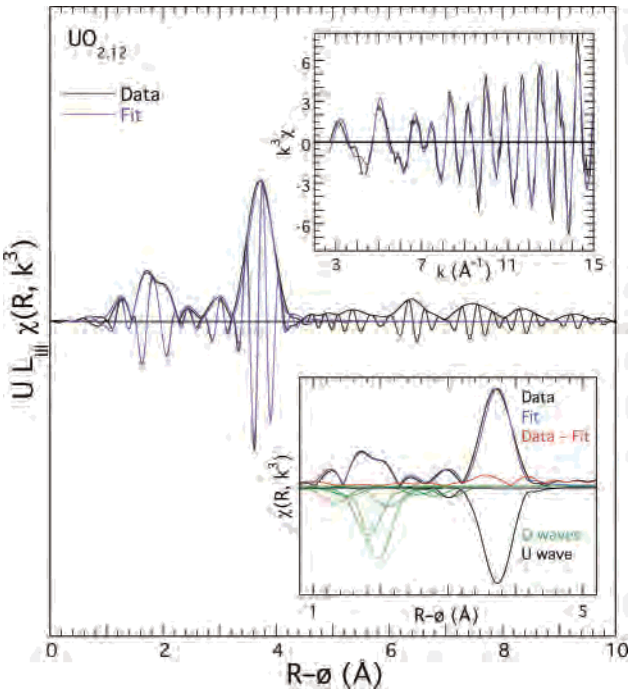

Figure 8. $k^3\chi(R)$ of the EXAFS of $UO_{2.12}$ and nine shell fit to the spectrum of $UO_{2.12}$. The layout is identical to Figure 6.

The curve fitting produced another trend. The total number of first shell O atoms begins just above 8 at low x, rises to 11.2 for $x = 0.08$, and then declines to 5.4 for $x = 0.20$. The cause of this can be found in the $\chi(R)$ representations of the curve-fits (Figures 5−10). When the primary O contribution is single peaked, it can be fit by a single O shell with U−O at 2.36 Å with only some additional small shells with U−O of 1.96 and 2.55 Å required to fit the features on the margins. However, when the primary O contribution becomes more complex at $x = 0.08$ then the peak at $R =$

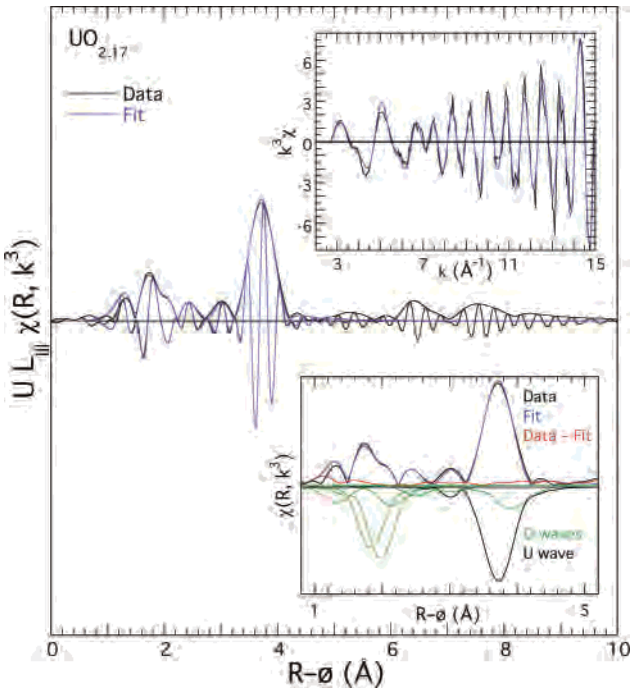

Figure 9. $k^3\chi(R)$ of the EXAFS of $UO_{2.17}$ and eight shell fit to the spectrum of $UO_{2.17}$. The layout is identical to Figure 6.

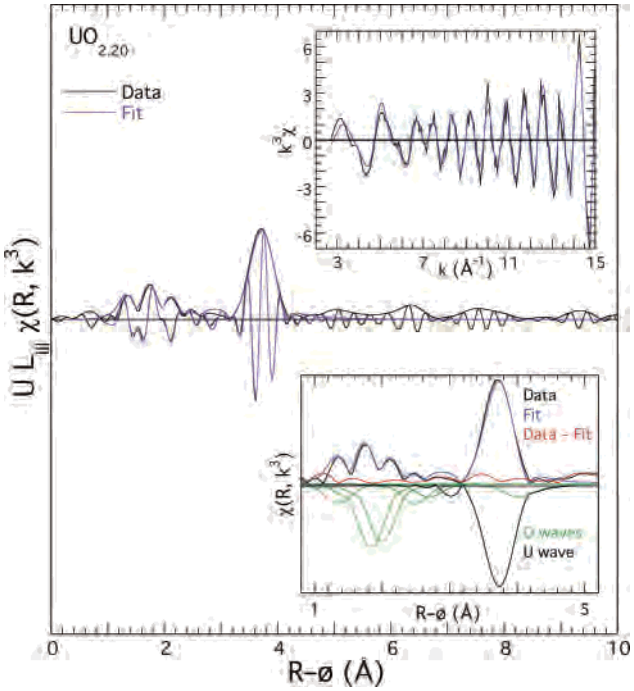

Figure 10. $k^3\chi(R)$ of the EXAFS of $UO_{2.20}$ and seven shell fit to the spectrum of $UO_{2.20}$. The layout is identical to Figure 6.

1.6 Å must be fit by a separate shell with U−O near 2.25 Å (Table 2). Because of interference, the amplitude of the contribution of the crystallographic shell with U−O near 2.38 Å must be much larger than the feature at $R = 2.0$ Å in the spectrum, requiring another large O contribution with U−O near 2.55 Å to reduce the amplitude and obtain a good fit on the high R side of the main peak. As x increases, the overall numbers decrease to match the rapid diminution of the primary O contribution even as their size relative to the O peak remains large. Progressively fewer shells are subsequently needed to complete the fit in the $R = 2.2-3.2$ Å region, suggesting that those shells near 2.8 and 3.2 Å found in only a limited number of fits may not be real or that they are broadened to below the detection limit in some spectra. Especially at low x, their overall contribution to the spectrum is small. The 2.95 Å shell is an exception to this behavior; some spectra clearly exhibit a separate feature that is fit by this shell. This feature is the one that changes on going from $x = 0.05$ to 0.08. The 3.5 Å shell improves the fit near the U feature at $R = 3.0$ Å; its absence in the $x = 0.20$ fit results in a significant residual in this region indicative of major changes in the structure at this composition. These two shells with U−O distances of 2.95 and 3.5 Å become more important as x increases, indicating that they are part of the U_4O_9 structure. The shell near 1.95 Å displays the opposite pattern: necessary at low x but vanishing at higher x. It was found to be correlated with the primary U−O wave and exhibited higher N when the O shell near 1.74 Å was included in the fit.

This leaves the O shell with the very short 1.74 Å U−O distance, corresponding to a contracted, nonbridging uranyl moiety. The problem in interpreting these results is that the number of atoms found in this shell does not increase with increasing x but tends to remain constant. This can be understood by noting that the large values of N for $x = 0.05$ and 0.08 are most likely artifacts of the large amplitude of the primary O contribution that amplify the side lobe that overlaps with (or gives the frequency fit by) this O shell. This can be seen in the fits of the spectra with low x, where, relative to the high x spectra, the spectral feature near $R = 1.3$ Å in the data is overshot and otherwise poorly fit by the contribution of this shell. It is unlikely that the feature originates in an actual U−O wave at this distance and confirms the interpretation that is simply a sidelobe that coincidentally supports such a wave in the fit. It was also found that the inclusion of the O shell at 1.95 Å resulted in larger N for the 1.74 Å shell, so that the relatively constant N correlates with the diminishing size of the more distant shell. For larger x, however, inspection of the $\chi(R)$ curve-fits clearly shows that the numbers found are accurate relative to each other. We conclude that a uranyl oxo type moiety is definitely part of the structure for some range of compositions beginning below $x = 0.20$ and that it is not present or contains a much smaller number of atoms at $x = 0$.

Analysis of U Disorder. The reduction in the amplitude of the primary O contribution is easily understood as the transformation from a single to multisite U−O distribution with increasing x, which is at least qualitatively consistent with the crystallographic results. Similar behavior for the peak representing the U contribution may be more difficult to understand. The group that has been most assiduous in crystallographic characterization of the U−O system has made the point repeatedly that a characteristic of the U−O system is the conservation of the U sublattice with only limited lattice distortions across the entire composition range.[7,9,11,12,23] In contrast, a separate crystallographic analysis of U_4O_9[22] and earlier EXAFS studies[20] report evidence for significant disorder. This discrepancy may simply be a matter

of degree, but it is also an important aspect in the complementarity of diffraction and local structure measurements where the former are sensitive to the long-range average structure of the periodic/coherent portion of the material and the latter probe the short range order of all of the atoms in the sample.

Because of its significance vis-à-vis the UO_{2+x} problem and the fact that, unlike the U−O distribution, curve-fits find no evidence for multiple, resolved U shells even as the numbers of atoms in the single shell decrease by 80%, a more thorough investigation of the EXAFS was performed. This was based on a ratioing approach,[37] which is more direct than curve-fitting and allows for a more complete examination of the effects of data quality and other factors, e.g., anharmonicity, that could spuriously reduce the numbers of atoms found by the fits. The U−U wave can be separated from the $\chi(k)$ spectrum by subtracting all of the other waves of the fit from the original spectrum and extracting its amplitude function by Fourier filtering. Inspection of these amplitudes (Figure 11) shows that, just as in the $\chi(R)$ spectra, increasing x reduces their size. The amplitude envelopes are, for the most part, similar in shape. The reduction effect thus occurs across the entire range of the data so that it must involve changes in the numbers of U atoms and not only the Debye−Waller factors. The exceptions involve the lower amplitude spectra that are more susceptible to noise and the low k data where there is clearly a low-frequency contribution to the spectra that was not fit and that causes the filtered U−U amplitude to separate from the data.

Plotting the logarithm of the U−U amplitudes divided by this amplitude from the $x = 0$ spectrum against k^2 helps to deconvolute the number of atoms and Debye−Waller factor contributions to the amplitude because of their different functional forms. If the amplitude functions are identical, as they should be in this case where chemical transferability is not an issue, then they would be straight lines whose intercept gives the change in the number of atoms and whose slope gives the difference in σ. Least-squares fits to lines eliminate the effects of noise and allow the ratio to be extrapolated to the intercept. When this sequence of operations is performed, it is evident (Figure 11) that the most consistent and important influence on the amplitude reduction seen in the spectra and found in the curve-fits is a loss of neighboring atoms and not an increase in σ. Since the structural transformations do not involve a change in the number of atoms in the near neighbor U shell and the compounds apparently remain close to full density, the location of these missing atoms is not obvious.

A set of simulations was therefore performed in which the effect of broadening the U−U distribution on the ln(ratio) was determined. Symmetric distributions were used not only because displacements of atoms in the lattice tend to be mirrored but also because asymmetric ones increase the Debye−Waller factors, an effect that was not observed in these data. Dividing the U atoms into three subshells with a

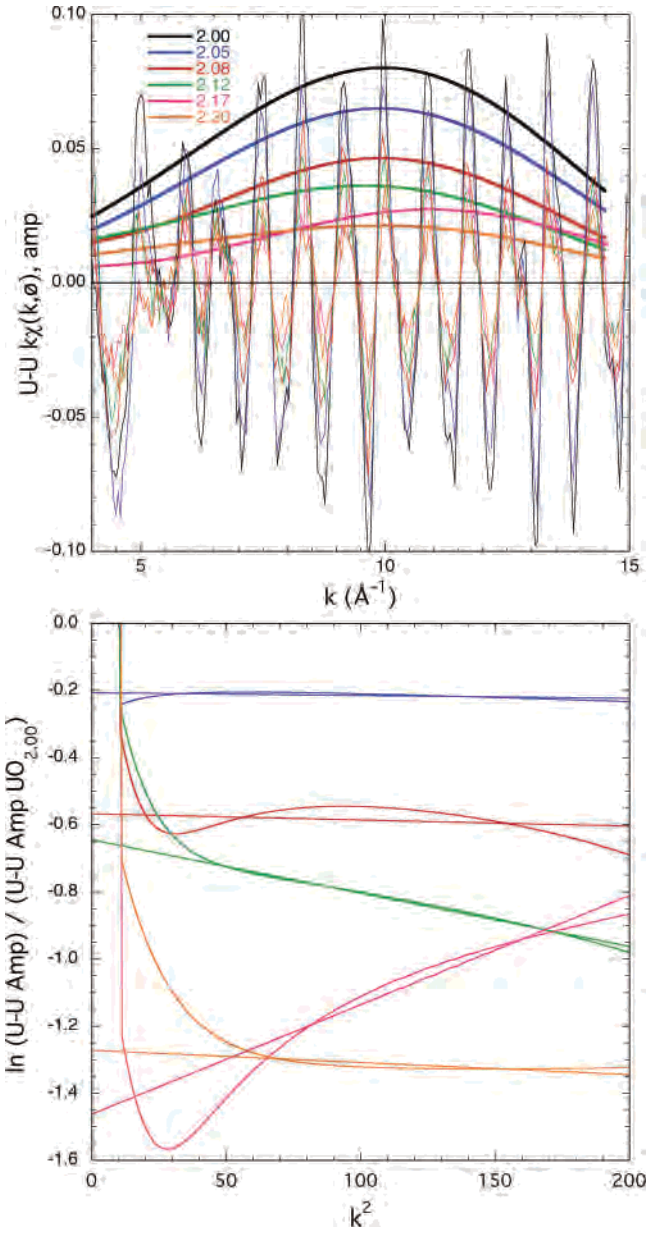

Figure 11. Upper: U−U $k^3\chi$ spectra from indicated samples, obtained by subtracting all U−O components of fit from spectrum, and corresponding amplitudes obtained by Fourier filtering these waves. The data contain additional contributions from unfit structural components, especially at low k. As the amplitude diminishes with increasing x the relative error will be amplified. Lower: Logarithms of the ratios of the U−U amplitudes from above with that from the $U_{2.00}$ U−U amplitude. Half the slope is the difference in σ^2, and the intercept is the ratio of the number of atoms times the reciprocal of the squares of the distances. The number of atoms is clearly decreasing with increasing x even while changes in σ are relatively small.

1:2:1 occupancy ratio and then symmetrically increasing the separation between them through the resolution limit resulted in a large loss of amplitude that the ratioing approach showed (Figure 12) was solely the result of an increase in σ. The only means of reducing the overall amplitude and giving an apparent reduction in the number of atoms was to spread the atoms out over > 0.4 Å and divide them into more shells, dispersed so that the individual ones are not resolved (Figure 13). Doing so produces a combination of an ordered and a glassy distribution. The ordered fraction remains very much like $UO_{2.00}$, with no change in the U−U distance or trend in

(37) Teo, B. K. *EXAFS: Basic Principles and Data Analysis*; Springer-Verlag: New York, 1986.

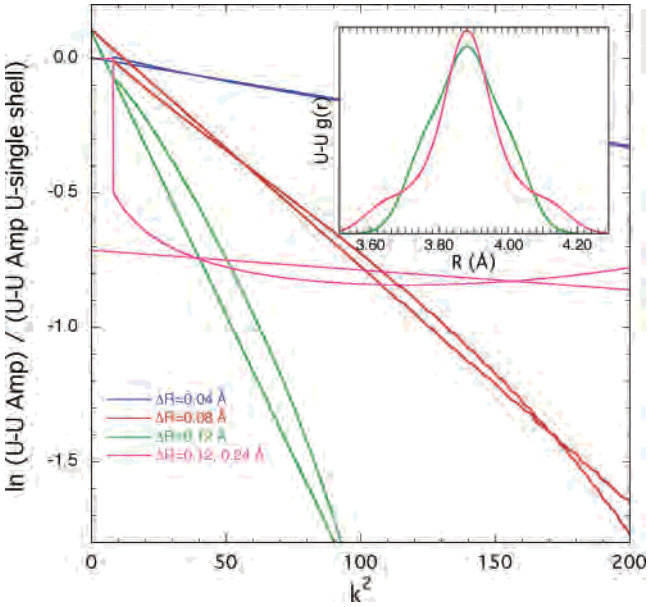

Figure 12. As in Figure 11, for the EXAFS calculated from different calculated U−U distributions. In the first three, the distribution is composed of three shells with a 1:2:1 ratio in the numbers of their atoms, $\sigma = 0.06$ Å, the center shell positioned at 3.88 Å, and the separations indicated, which gave the distribution depicted in the inset for the 0.12 Å separation. It can be seen that, with this type of distribution, even past the resolution limit of the data range used, the total number of atoms given by the intercept remains almost constant and the increased separation is reflected solely in larger values of σ. Reducing the apparent numbers of atoms can be seen to require a distribution consisting of an ordered part (7 atoms at 3.88 Å) and a glassy part in which the atom density changes only slowly over almost 0.5 Å (1 atom each at ±0.24 Å and 1.5 atoms each at ±0.12 Å around the center, all σ's = 0.06 Å). This type of distribution also produces only a minimal increase in the apparent σ, and thus duplicates the behavior of the actual data from Figure 10.

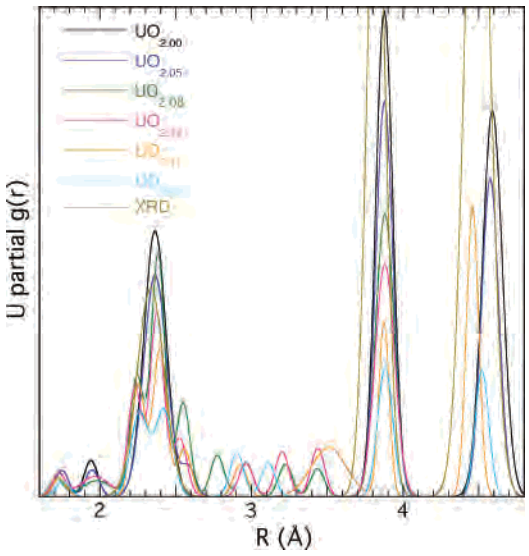

Figure 13. U partial $g(r)$ or radial structure function from the UO_2 crystal structure and from the curve-fits for indicated samples. The peak near 3.8 Å is the U neighbor, and all others are O shells.

σ. The glassy component is apparently spectroscopically invisible and does not contribute to the EXAFS. The overall effect is therefore to reduce the total number of atoms with only minimal changes in σ relative to its value in the ordered portion, the behavior observed in the spectra. This indicates that not only must the missing fraction of the U atoms disorder so as to produce a range of distances at least several tenths of an Å in extent but also that they must do so continuously relative to the thermal widths of the individual sites.

Discussion

It has been emphatically stated that throughout the oxidation of UO_2 to UO_3 the added O atoms are not distributed randomly but are incorporated as ordered structures in domains that gradually enlarge and merge until they become the new host.[7,9,11,23] This mechanism produces nanophase separation and, since both structures are ordered, heterogeneity on this same scale. The observation that the UO_2 extended structure simply diminishes evenly throughout the spectrum rather than vanishes from longer distances inward corroborates this. Describing this material as composed of nanoscale domains can easily be rationalized by understanding that the energetics of a given domain will be heavily influenced by its size, shape, interfaces, and entropic effects. Nanoscale heterogeneity would also result in a wide range of local oxidation potentials for nominally identical structures and provide a context for other attributes of this material. It is also consistent with photoemission that was interpreted as corroborating the Willis structure model that includes multiple types of U sites that begin with UO_2 and extend through higher valences.[38]

The most appealing aspects of the multisite U−O distribution are those that give separate features in the spectra of the compounds with high x. These are the splitting of the primary O shell in two shells with U−O of 2.25 and 2.40 Å, the O shells near 3.45, 3,20, and 2.95 Å, and the O shell at the very short 1.74 Å distance. The O shells at 1.96 and 2.55 Å may improve the fits at the margins of the primary O contribution and thus reflect asymmetry or other kinds of disorder that alter the shape at certain values of x but are not distinct neighbor atom shells. Alternatively, they could belong to intermediate phases as just described. The actual distributions may thus differ somewhat than those obtained from the curve-fits (Figure 13), with the features broadened and overlapping more than depicted. The rdf's (Figure 13), and curve-fit parameters from which they are calculated, are therefore best considered as a schematic, indicating trends rather than literal behavior, especially insofar as they are attempting to describe a complicated mixture in transition. The total numbers of O nearest neighbors are unlikely to change by much, certainly not by the amounts or even necessarily directions obtained from the curve-fits. It is the broadening of the primary O distribution by a shift of a significant number of the O atoms to around 2.25 Å and the anharmonic and glassy parts that develop as part of this process that cause the decrease in number of O atoms found by the fits. The changes in the XANES therefore signify this continuous decrease in short range order, involving the U as well as the O shells. In addition to this disordering of the primary shells, the extra O atoms cause larger O displace-

(38) Allen, G. C.; Tucker, P. M. Tyler, J. W. *J. Chem. Soc., Chem. Commun.* **1981**, 691.

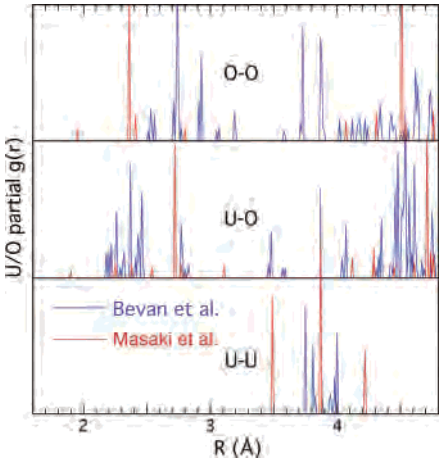

Figure 14. Partial $g(r)$'s or radial structure functions for U_4O_9 calculated from the two crystal structures. That of Masaki et al. does not include the UO_2 portion of the lattice but only the disordered fraction.

ments to give shells at intermediate distances up to 3.5 Å. These can be compared with the distributions obtained from the two crystal structures of U_4O_9 (Figure 14) and with the 2.28−2.34, 2.81, and 3.23 Å distances calculated for U_3O_7.[12]

This more recent crystal structure appears to correspond well with the primary O distribution, which widens to include distances ranging from 2.15 to 2.45 Å with new peaks around 2.26 and 2.48 Å that are reasonably close to the 2.25 and 2.55 Å U−O distances found by the EXAFS. The older structure shows far fewer O atoms involved at a smaller number of distances, but these locations are somewhat closer to those obtained here. Its largest O peak from the disordered portion of the compound occurs near 2.74 Å, with the newer structure giving U−O distances in this region that are closer to the shell at 2.94 Å from the EXAFS. Beyond this, the older structure also shows a U−O distance near 3.12 Å while the newer one gives a set between 3.45 and 3.6 Å with a peak just below 3.5 Å. The EXAFS therefore indicates that aspects of both structures are generally correct but also that a combination of both is needed to describe all of the shells. Similarly, the 0.25 Å width of the U−U distribution from the newer structure is far too narrow to account for the loss of U amplitude. The 0.7 Å width of the older structure is much closer to these EXAFS results in this respect, but it failed to identify any intermediate distances required to give the continuous distribution indicated here. A combination of the two would again appear to be more consistent with the EXAFS. U_3O_7 has U−O distances that also fall within this range, below 2.3 Å, at 2.8 Å, and 3.2−3.3 Å. These distances are in general agreement with those found in at least some samples but fail to account for all of the U−O distances observed.

The vital question of the short, uranyl oxo-type distance and the charge distribution mechanism remains. The older U_4O_9 structure includes a 1.92 Å uranyl−uranate oxo distance, which agrees in principle but still differs from our EXAFS distance by almost 0.2 Å. The group that has performed the most recent U_4O_9 structure determination as well as those of many more phases in this system has never identified a U−O distance <2.2 Å, either crystallographically or by EXAFS. Crystallography, however, is sensitive to the periodic components in the arrangement of atoms, and as we have recently demonstrated,[39] the signatures of locally ordered structures that are distributed aperiodically or incoherently can be quite subtle even in the diffuse component of the scattering. Their XAFS measurements[20] were performed on a more limited set of samples that did not encompass the almost continuous change in stoichiometry presented here that greatly facilitates the identification of small changes in the structure. In addition, their analysis was complicated by noisier data over a more limited range and its use of a difference method to characterize non-UO_2 components that is not well suited to locally disordered systems. In this current study, the presence of some oxo-type moieties is unequivocal at higher values of x. The behavior of the fits at low x indicates fewer or zero oxo groups near $UO_{2.00}$.

If oxo-type atoms are absent, then the additional charge must either reside on the O as peroxide, be delocalized over many U atoms with fractionally larger charge, or both. Some relatively short O−O distances suggest that some of the former mechanism is in effect. Applying Zachariasen's Valence Shell Bond method[15] analogously to its use for uranates[14] shows, however, that the latter mechanism, delocalization of charge, would dominate. In the 222 and 432 type of defects, the rotation around the octahedral holes and subsequent displacement that produces the O′ type atoms shortens the two U−O distances to each U atom by around 0.16 Å, enough to raise the total charge on each by just under one-half. The two U atoms below the O″ each have one short U−O distance, raising their charge by around 0.1 each, but the U atoms just above and below the O″ atoms in the planes with the O′ pair are now 9-coordinate and their charge is raised by close to 1.4 because of the three O defect atoms. It must then be asked if this coordination geometry, 6 O at 2.37 Å, 1 at 2.29 Å, and 2 at 2.21 Å, is feasible.

This coordination geometry would not only be unique in U coordination chemistry but also has no precedent in a single phase crystal structure, assuming that the EXAFS results herein are correct and the U_4O_9 structures actually contain UO_2- and U_3O_7-type nanodomains within the host U_4O_9 phase. The average U−O distances in 8−10-coordinate mononuclear U(IV) complexes are >2.4 Å and would appear to be limited by steric constraints and the O−O separation. Symmetric uranates stabilize U(VI) with six O near 2.15 Å; asymmetric uranates are stabilized by taking on an oblate geometry with the trans dioxo configuration and 4−5 ligands at a much longer distance in the equatorial plane (in coordination chemistry the higher numbers occur only with bidentate ligands).[13] This increase in charge always occurs in parallel with a contraction of at least some bonds and a reduction in the number of ligands. The U(VI)−oxo moieties implied by the 1.74 Å U−O distances are appealing because they are so well precedented. Therefore, is it more likely that the recent crystal structure on this disordered compound missed the oxo groups or that these EXAFS results are

(39) Garcia-Adeva, A. J.; Conradson, D. R.; Villella, P.; Conradson, S. D. *J. Phys. Chem. B* **2003**, *107*, 6704.

erroneous and that the 9-coordinate U with U−O distances of 2.21−2.37 Å is a stable configuration?

In addressing this question, these results for UO_{2+x} can be compared with our recent study of PuO_{2+x}.[5,35] The presence of oxo groups and their correlation with x is even more unequivocal for Pu because the Pu system displayed an effect not observed here. Intrinsic, stable disorder in the primary O shell associated with the possible substitution of the O^{2-} ions by OH^- and related H_2O hydrolysis species reduces the amplitude of the primary O shell to a low value more often than observed in UO_{2+x} and enhances the visibility of the oxo shell in more cases. Another difference between the two systems is the 0.15 Å shorter U−oxo distance relative to the Pu−oxo ones. For the former, this would imply U(VI) with oxo groups that is even more chemically isolated from their environments than in normal uranyl complexes. The 1.83−1.90 Å bond lengths in the latter not only imply Pu(V) but also suggest that the oxo groups might be bridging. The oxo groups for both U and Pu also differ from those in solution in that the distances from the oxo atoms to neighboring cations are less than 2.4 Å so that it is not clear how comparable they are to the more conventional type. Perturbations of the electronic structure could promote unusual types of geometries,[40] such as mono-oxo,[41] that exhibit shorter U−O bonds that would have significant implications for the extended structure. It is pointed out that the adoption of the normal geometries associated with higher valence oxo-containing moieties in PuO_{2+x} automatically created additional short Pu−O distances in adjacent Pu sites. The problem this creates for UO_{2+x} is that these U−O distances, shorter by 0.15 Å, diminish the total coordination numbers associated with the V and VI valences, whereas the reactions involve an increase in the total number of O atoms in the compound. A corollary to an O incorporation mechanism that involves oxo atoms is therefore that some U−O distances are substantially increased with concomitant reduction of the number of U atoms that they bridge so as to decrease the U total coordination numbers. The different mechanisms of oxo bonding and incorporation may also be the source of the slight expansion of the lattice constant of PuO_{2+x} with increasing x[4] whereas UO_{2+x} undergoes a decrease.[2,3] One explanation of this difference is that Pu is already minimally sized at $PuO_{2.00}$, so that the extra O atoms can only swell the lattice, whereas U is not and the extra O contracts the U atoms.

This study demonstrates that the structures and chemistry of the AnO_{2+x} systems remain open and exciting. Despite ostensible similarity in their behaviors, there are significant differences in the structure and chemistry of AnO_{2+x} as An ranges from U to Pu.

Acknowledgment. All experimental measurements were performed at the Stanford Synchrotron Radiation Laboratory, a national user facility operated by Stanford University on behalf of the U.S. Department of Energy, Office of Basic Energy Sciences. Health Physics support was provided by the Los Alamos National Laboratory branch of the Seaborg Institute for Transactinium Science. This work was supported by the NNSA and OBES Division of Chemical Sciences under Contract W-7405.

IC049748Z

(40) Denning, R. G. *Struct. Bonding* **1992**, *79*, 215.
(41) De Wet, J. F.; Du Preez, J. G. H. *J. Chem. Soc., Dalton Trans.* **1978**, 592. O'Grady, E.; Kaltsoyannis, N. *J. Chem. Soc., Dalton Trans.* **2002**, 1233.